A STUDY OF INITIAL AND BOUNDARY CONDITIONS FOR SPATIALLY DEVELOPING PLANAR MIXING LAYERS

Renan de S. Teixeira, renanpcivil@yahoo.com.br
Leonardo S. de B. Alves, leonardo_alves@ime.eb.br
Programa de Pós-Graduação em Engenharia de Defesa, Instituto Militar de Engenharia, Rio de Janeiro, Brazil

Abstract. *The current paper presents a numerical study on a bounded domain of spatially developing incompressible planar mixing layers. This flow represents a free shear layer that is already convectively unstable at very low Reynolds numbers. In such cases, small perturbations are amplified as they propagate downstream. Simplified conditions have to be used instead of the governing equations themselves at the artificial boundaries created for this originally unbounded problem. Hence, undesirable numerical waves are created as vortex structures propagate outwards. They propagate upstream and are reflected back into the domain by the inflow boundary, mimicking an impulse excitation that shouldn't exist. This numerical forcing mechanism generates new vortex structures, and the entire process is repeated. The main goal of this paper is to propose a procedure to minimize this problem. It starts with dual-time-stepping to introduce a physical-time derivative in any arbitrary code, where the original time derivative assumes the role of a pseudo-time derivative. The new unsteady term is then approximated with an implicit Euler scheme, where the amount of numerical dissipation added can be properly adjusted through the physical-time step. This procedure damps all numerically induced waves and allows the generation of artificial steady-state solutions for any Reynolds number without further distortions of spatial gradients. A direct consequence is that all steady profiles generated have the same spatial accuracy originally designed for the arbitrary code utilized. They can be used as accurate initial conditions and/or reference solutions for boundary conditions in physical-time accurate simulations performed with the original code.*

Keywords: *Artificial Dissipation, Boundary conditions, Planar Mixing-layers, Spatially Developing Flows*

1. INTRODUCTION

Spatially developing incompressible planar mixing layers represents a free shear layer that is already convectively unstable at very low Reynolds numbers. In such cases, small perturbations are amplified as they propagate downstream. The first coherent structure formed in a transient simulation is the startup vortex. Many authors claim that a first derivative discontinuity between initial and inflow conditions is responsible for its formation (Buell and Huerre, 1988). In the absence of external excitations, the flow should relax to its steady-state solution.

On the other hand, numerical simulations of external flow problems pose one of the most difficult challenges in computational fluid mechanics because the original unbounded domain must be limited to a bounded one. Hence, simplified boundary conditions have to be implemented instead of the governing equations themselves at the artificial boundaries created. As the flow exits through the boundaries, undesirable numerical waves are reflected back into the bounded domain and create numerically induced impulse-like perturbations at the inlet, which acts as a nonphysical noise source.

An alternative solution to this problem is coordinate transformation, i.e., mapping the unbounded domain into a bounded one before attempting a numerical solution of the respective governing equations (Grosch and Orszag, 1977). However, the loss of implicit resolution in the mesh introduces undesirable numerical oscillations when the flow does not relax smoothly to its boundary condition at infinity.

Two types of high accuracy artificial boundary conditions can be found in the literature. The first type includes global boundary conditions, which require a finite region that extends away from the boundary to be effective (Blaschak and Kriegsmann, 1988; Bodony, 2006). Stretched meshes, commonly used to introduce dissipation in the far field, can be considered a subset of this group. They also allow the artificial boundaries to be placed far from the region of interest without substantially increasing mesh size. Furthermore, they are often used with absorbing boundary conditions. This method introduces a source term in conservation equations that force the computed solution to converge towards a reference solution near the artificial boundary. Thus, undesirable numerical waves are damped before actually reaching this boundary.

The other type includes local boundary conditions, which only act on the artificial boundary controlling the inflow and outflow of waves crossing it. One widely used subset is known as non-reflective boundary conditions. They model the behavior of linear perturbations around a reference solution at the boundary (Giles, 1990; Colonius et al, 1993) in order to minimize reflections. Another popular subset is known as characteristic boundary conditions, which are based on variations of the local one dimensional inviscid (LODI) relations (Thompson, 1987; Poinsot and Lele, 1992) . This method prevents the characteristic waves coming from outside the truncated domain to enter it, minimizing unwanted numerical reflections.

The methods briefly described above are represent the state of the art for numerical simulations of compressible flows. In order to extend these formulations to transient compressible flows at low Mach numbers, the dual-time step

preconditioning method is employed (Venkateswaran et al, 2002). The current paper is an extension of previously reported works (Alves, 2006; Teixeira et al, 2008), where all spatial derivatives were approximated with second-order central differences on a non-uniform mesh, with scalar artificial dissipation applied for the inviscid fluxes. Furthermore, an approximate hyperbolic tangent function was used as initial condition and the original LODI relations were used at both inlet and outlet boundaries. The present paper reports results obtained with an extended version of this code, which is now fourth-order accurate in space, that utilizes improved initial and boundary conditions to further minimize numerical errors.

2. MATHEMATICAL EQUATIONS

The two-dimensional preconditioned governing equation are

$$\mathbf{\Gamma}\frac{\partial\hat{\mathbf{Q}}}{\partial\tau}+\frac{\partial}{\partial x}(\mathbf{E}_i-\mathbf{E}_v)+\frac{\partial}{\partial y}(\mathbf{F}_i-\mathbf{F}_v)=\mathbf{H}\ , \tag{1}$$

with primitive and conservative variables given by

$$\hat{\mathbf{Q}}=(p_g,u,v,T,Y_1)^T \quad \text{and} \quad \mathbf{Q}=(\rho,\rho u,\rho v,\rho E,\rho Y_1)^T\ , \tag{2}$$

respectively, with ρ standing for density, p for pressure, u and v for the Cartesian velocity components, e for thermal internal energy, $E=e+(u^2+v^2)/2$ for total internal energy, Y_1 for mass fraction of the first specie within a two species mixture. The inviscid and viscous fluxes $\mathbf{E}_i$, $\mathbf{F}_i$, $\mathbf{E}_v$ and $\mathbf{F}_v$ have a standard definition and $\mathbf{H}$ represents the source term. Further details about the differential model used here can be found elsewhere (Teixeira et al, 2008).

2.1 Temporal Discretization

Two different approaches must be used for the time derivatives since we employ a dual-time-step methodology. First, the pseudo-time derivative is approximated by the implicit Euler scheme with an uniform pseudo-time step $\Delta\tau$,

$$\frac{\partial\hat{\mathbf{Q}}}{\partial\tau}\simeq\frac{\Delta\hat{\mathbf{Q}}}{\Delta\tau}+O(\Delta\tau)\ , \tag{3}$$

where $\Delta\hat{\mathbf{Q}}=\hat{\mathbf{Q}}^{p+1}-\hat{\mathbf{Q}}^{p}$ is the pseudo-time increment or residue and p is the pseudo-time index, since our goal is fast convergence towards pseudo-time steady-state and accuracy in pseudo-time not needed. The physical-time derivative is approximated by a multi-step backward difference formula (BDF) with nonuniform physical-time steps,

$$\frac{\partial\mathbf{Q}}{\partial t}\simeq\hat{a}_{N_t}\mathbf{Q}^{n+1}+\sum_{i=0}^{N_t}a_{N_t,i}\mathbf{Q}^{n-i}+O(\Delta t^{N_t+1})\ , \tag{4}$$

where n is the physical-time index and $N_t=0$ for the first physical-time iteration, $N_t=1$ for the second iteration, and so on up to the global accuracy-order required for the remaining steps. Coefficients $\hat{a}_{N_t}$ and $a_{N_t,i}$ in expression above are given in Table 1 shown below.

Table 1. Physical-time Coefficients Derivative

	$N_t=0$	$N_t=1$	$N_t=2$
$\hat{a}_{N_t}$	$\frac{1}{t_{n+1}-t_n}$	$\frac{1}{t_{n+1}-t_{n-1}}+\frac{1}{t_{n+1}-t_n}$	$\frac{1}{t_{n+1}-t_{n-2}}+\frac{1}{t_{n+1}-t_{n-1}}+\frac{1}{t_{n+1}-t_n}$
$a_{N_t,0}$	$-\frac{1}{t_{n+1}-t_n}$	$-\frac{t_{n+1}-t_{n-1}}{(t_{n+1}-t_n)(t_n-t_{n-1})}$	$-\frac{(t_{n+1}-t_{n-2})(t_{n+1}-t_{n-1})}{(t_{n+1}-t_n)(t_n-t_{n-2})(t_n-t_{n-1})}$
$a_{N_t,1}$	0	$\frac{t_{n+1}-t_n}{(t_{n+1}-t_{n-1})(t_n-t_{n-1})}$	$\frac{(t_{n+1}-t_{n-2})(t_{n+1}-t_n)}{(t_{n+1}-t_{n-1})(t_n-t_{n-1})(t_{n-1}-t_{n-2})}$
$a_{N_t,2}$	0	0	$-\frac{(t_{n+1}-t_{n-1})(t_{n+1}-t_n)}{(t_{n+1}-t_{n-2})(t_n-t_{n-2})(t_{n-1}-t_{n-2})}$

Equation (1), in its discrete form in both pseudo-time and physical-time, then becomes

$$\mathbf{\Gamma}^p\frac{\hat{\mathbf{Q}}^{p+1}-\hat{\mathbf{Q}}^{p}}{\Delta\tau}+\hat{a}_{N_t}\hat{\mathbf{Q}}^{p+1}+\sum_{i=0}^{N_t}a_{N_t,i}\mathbf{Q}^{n-i}+\frac{\partial}{\partial x}(\mathbf{E}_i-\mathbf{E}_v)^{p+1}+\frac{\partial}{\partial y}(\mathbf{F}_i-\mathbf{F}_v)^{p+1}=\mathbf{H}^{p+1}\ , \tag{5}$$

where the latest physical-time and pseudo-time steps, $n+1$ and $p+1$, respectively, were assumed equal for all variables. This approximation is necessary for dual-time-step methods that employ multi-step schemes in physical-time in order to guarantee that a physical-time accurate discrete equation is recovered at pseudo-time steady-state.

In order to construct an implicit time marching scheme, equation (5) needs to linearized. Hence, a Taylor series of an arbitrary vector $\mathbf{f}$, as follows,

$$\mathbf{f}^{p+1} \simeq \mathbf{f}^p + \left.\frac{\partial \mathbf{f}}{\partial \tau}\right|^p \Delta\tau + O(\Delta\tau^2) \simeq \mathbf{f}^p + \left(\frac{\partial \mathbf{f}}{\partial \hat{\mathbf{Q}}}\frac{\partial \hat{\mathbf{Q}}}{\partial \tau}\right)^p \Delta\tau + O(\Delta\tau^2) \simeq \mathbf{f}^p + \left.\frac{\partial \mathbf{f}}{\partial \hat{\mathbf{Q}}}\right|^p \Delta\hat{\mathbf{Q}} + O(\Delta\tau^2) \ , \tag{6}$$

must be employed, where $\partial\mathbf{f}/\partial\hat{\mathbf{Q}}$ represents all but one of the possible Jacobians out of equation (5). The inviscid preconditioned Jacobians $\hat{\mathbf{A}}$ and $\hat{\mathbf{B}}$ obtained from $\mathbf{f} = \mathbf{E}_i$ and $\mathbf{F}_i$, respectively, are given elsewhere (Teixeira et al, 2008), but the conservative to primitive dependent variable Jacobian $\mathbf{T} = \partial\mathbf{Q}/\partial\hat{\mathbf{Q}}$ is obtained from the linearization of $\mathbf{f} = \mathbf{Q}^{p+1}$. This Jacobian is similar to the preconditioning matrix $\mathbf{\Gamma}$, except the terms

$$\rho_P = \frac{\partial \rho}{\partial P} \quad , \quad \rho_T = \frac{\partial \rho}{\partial T} \quad \text{and} \quad \rho_{Y_i} = \frac{\partial \rho}{\partial Y_i} \ , \tag{7}$$

where these derivatives are obtained from the perfect gas relations in the present work.

The diffusive fluxes are linearized in a different way (Choi and Merkle, 1993; Shuen et al, 1993). Using $\hat{\mathbf{Q}}^{p+1} = \hat{\mathbf{Q}}^p + \Delta\hat{\mathbf{Q}}$, we can write

$$\left(\frac{\partial \mathbf{E}_v}{\partial x} + \frac{\partial \mathbf{F}_v}{\partial y}\right)^{p+1} \simeq \left(\frac{\partial \mathbf{E}_v}{\partial x} + \frac{\partial \mathbf{F}_v}{\partial y}\right)^{p} + \left(\frac{\partial}{\partial x}\mathbf{R}_{x,x}\frac{\partial}{\partial x} + \frac{\partial}{\partial y}\mathbf{R}_{y,y}\frac{\partial}{\partial y}\right)^p \Delta\hat{\mathbf{Q}} \ , \tag{8}$$

where formulation (8) would be exact if the cross diffusion Jacobians $(\mathbf{R}_{x,y}, \mathbf{R}_{y,x})$ were not neglected. The normal diffusion Jacobians are given by

$$\mathbf{R}_{x,x} = \begin{pmatrix} 0 & 0 & 0 & 0 & 0 \\ 0 & 3/4\mu & 0 & 0 & 0 \\ 0 & 0 & \mu & 0 & 0 \\ 0 & 3/4\mu u & \mu v & k & \rho(D_{e,1}, h_1)^* \\ 0 & 0 & 0 & 0 & \rho D_{e,1} \end{pmatrix} \quad \text{and} \quad \mathbf{R}_{y,y} = \begin{pmatrix} 0 & 0 & 0 & 0 & 0 \\ 0 & \mu & 0 & 0 & 0 \\ 0 & 0 & 3/4\mu & 0 & 0 \\ 0 & \mu u & 3/4\mu v & k & \rho(D_{e,1}h_1)^* \\ 0 & 0 & 0 & 0 & \rho D_{e,1} \end{pmatrix} \ , \tag{9}$$

where $(D_{e,1}h_1)^* = (D_{e,1}h_1 - D_{e,2}h_2)$.

Applying the linearization discussed above to equation (5), we obtain

$$\left\{\mathbf{S} + \Delta\tau\left(\frac{\partial}{\partial x}\left(\hat{\mathbf{A}}\cdot\right) + \frac{\partial}{\partial y}\left(\hat{\mathbf{B}}\cdot\right)\right) - \Delta\tau\left(\frac{\partial}{\partial x}\mathbf{R}_{x,x}\frac{\partial}{\partial x} + \frac{\partial}{\partial y}\mathbf{R}_{y,y}\frac{\partial}{\partial y}\right)\right\}^p \Delta\hat{\mathbf{Q}} = -\Delta\tau\,\mathbf{R}^p \ , \tag{10}$$

where $\mathbf{S}^p$ and $\mathbf{R}^p$ are written as

$$\mathbf{S}^p = \mathbf{\Gamma}^p + \Delta\tau(\hat{a}_{N_t}\mathbf{T} - \mathbf{D})^p \quad \text{and} \quad \mathbf{R}^p = \sum_{i=0}^{N_t} a_{N_t,i}\mathbf{Q}^{n-i} + \frac{\partial}{\partial x}(\mathbf{E}_i - \mathbf{E}_v)^p + \frac{\partial}{\partial y}(\mathbf{F}_i - \mathbf{F}_v)^p - \mathbf{H}^p \ , \tag{11}$$

with $\mathbf{D}$ representing the Jacobian for the source term $\mathbf{H}$, which is zero in the present work. It is important to note that equation (10) must be written in the incremental or residual form presented. In doing so, the pseudo-time steady-state solution generated will be independent of the pseudo-time step (Tannehill et al, 1984). This allowed the implicit Euler scheme chosen for pseudo-time marching to be optimized towards faster convergence rates without any accuracy constraint.

The solution of equations (10) and (11) is computationally expensive to invert due to the sparse nature of the implicit matrix on the left hand side of (10), which is block penta-diagonal, as shown later. In such cases, an approximate factorization of this implicit matrix must be used. We have done so with the **ADI** scheme, known as Alternating Direction Implicit scheme (Douglas and Gunn, 1964). Following this approach, equation (10) was approximately factored as

$$\left\{\mathbf{S} + \Delta\tau\left(\frac{\partial}{\partial x}\hat{\mathbf{A}} - \frac{\partial}{\partial x}\mathbf{R}_{x,x}\frac{\partial}{\partial x}\right)\right\}^p \mathbf{S}^{-1}\left\{\mathbf{S} + \Delta\tau\left(\frac{\partial}{\partial y}\hat{\mathbf{B}} - \frac{\partial}{\partial y}\mathbf{R}_{y,y}\frac{\partial}{\partial y}\right)\right\}^p \Delta\hat{\mathbf{Q}} = -\Delta\tau\,\mathbf{R}^p \ , \tag{12}$$

which is then solved in two steps,

$$\left\{\mathbf{S} + \Delta\tau\left(\frac{\partial}{\partial x}\hat{\mathbf{A}} - \frac{\partial}{\partial x}\mathbf{R}_{x,x}\frac{\partial}{\partial x}\right)\right\}^p \Delta\tilde{\mathbf{Q}} = -\Delta\tau\,\mathbf{R}^p \quad \text{and} \tag{13}$$

$$\left\{\mathbf{S} + \Delta\tau\left(\frac{\partial}{\partial y}\hat{\mathbf{B}} - \frac{\partial}{\partial y}\mathbf{R}_{y,y}\frac{\partial}{\partial y}\right)\right\}^p \Delta\hat{\mathbf{Q}} = \mathbf{S}\,\Delta\tilde{\mathbf{Q}} \ , \tag{14}$$

containing block tri-diagonal matrixes, much less computationally intensive to solve compared to the matrix associated with equation (10). This increase in efficiency comes at a cost: equations (10) and (12) are not equal. However, the left-hand size in both equations becomes as close to zero as arbitrarily prescribed by the stopping criteria imposed for the march in pseudo-time, and these systems of equations yield approximately the same solution.

2.2 Spatial Discretization

An existing code (Teixeira et al, 2008) was extended to approximate all spatial derivatives with fourth-order central difference schemes on nonuniform meshes. Scalar artificial dissipation for inviscid fluxes was introduced through a sixth-derivative at the explicit level and a second-derivative at the implicit level. They were chosen to be different in order to maintain the implicit matrix on the left-hand-side block tri-diagonal for efficiency purposes. Hence, they also used second-order accurate central differences for consistency. It is important to note that upon pseudo-time convergence at each physical-time step, the implicit side vanishes and the explicit side accuracy is recovered. Furthermore, accuracy-order was reduced at the boundaries to increase overall numerical stability.

Standard artificial dissipation formulas cannot be used within a preconditioned framework without making some adjustments. These formulas have to be changed because we are iterating our scheme in pseudo-time and not in physical time. Hence, the amplitude of the dissipation terms is affected. The formulation used is written by the following way

$$\mathbf{AD}_x = \epsilon_x^m \Delta x^{m-1} \mathbf{\Gamma} \lambda_x^+ \frac{\partial^m \hat{\mathbf{Q}}}{\partial x^m} \ , \tag{15}$$

for both explicit and implicit terms, where m is the derivative order and λ_x^+ is the highest eigenvalue. A similar formula was used to $\mathbf{AD}_y$. The coefficients ϵ were adjusted during validation runs to eliminate spurious oscillations without smoothing out spatial gradients.

3. RESULTS AND DISCUSSION

The main goal of the present work is to generate steady-state solutions that will be used in future simulations as reference profiles for initial and boundary conditions. For that reason, a first-order BDF is employed for physical-time marching instead of removing the physical-time derivative altogether, which is a more efficient way of generating steady-state solutions (Zeng et al, 2003). Furthermore, it does so without affecting spatial gradients since dissipation is introduced through a term that vanishes at steady-state.

Momentum thickness and velocity ratio are specified first because they determinate the hyperbolic tangent profile utilized as reference profile. These two parameters also impose the domain length for the subsequent simulations. The planar mixing layer is formed when two streams with different speeds meet downstream of a splitter plate. Here, the maximum streamwise velocity of lower stream is given by $U_1 = 0.34605\ m/s\ (Re_{1,\theta_0} \simeq 67,87)$, whereas the maximum streamwise velocity of the upper stream is $U_2 = 0.173025\ m/s\ (Re_{2,\theta_0} \simeq 33,94)$. Inlet momentum thickness is described by the follow equation

$$\theta_0 \ = \ \int_{-\infty}^{\infty} \left(\frac{1}{4} - \left(\frac{u(x=0,y) - \bar{U}}{U_1 - U_2} \right)^2 \right) dy \ = \ 0.316488\, mm \tag{16}$$

where $\bar{U} = (U_1 + U_2)/2$ with $U_1/U_2 = 0.5$. Linear stability analysis determines the disturbance wavelength and spatial growth rate as functions of frequency (or Strouhal number). In other words, it enables one to extract the frequency associated with the highest growth rate and extract the respective disturbance period and wavelength. According to the linear stability analysis, the most amplified linear disturbances under these conditions should propagate with a period of $\tau_{LSA} = 0.34827\, s$ and wavelength of $\Lambda_{AEL} = 0.09042\, m$. The streamwise domain length is set to approximately 10 wavelengths. On the other hand, the cross-stream domain width is approximately $100\,\theta_0$ in both directions, giving it a total width up to about $200\,\theta_0$ (Grinstein et al, 1990).

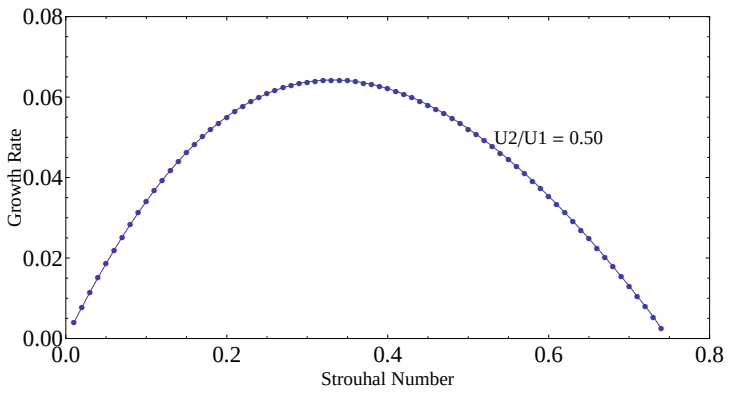

Figure 1. Mixing layer growth rate as a function of the Strouhal number for $U_1/U_2 = 0.5$ (Alves, 2006).

Inlet profiles were extended to the rest of the domain in order to compose the initial condition of all simulations. Inlet and outlet as well as side boundary conditions follow a standard implementation (Teixeira et al, 2008). Furthermore, spatial accuracy was secured by grid refinement, clustering grid points inside the mixing layer. Grid stretching away from the inlet boundary was also utilized when necessary. Figure 2 shows two meshes that use $N_X = 135$ and $N_Y = 122$ points in their respective directions, with and without the aforementioned stretching. Resolution studies were performed by increasing the number of grid points in both directions until no more changes were observed at steady-state.

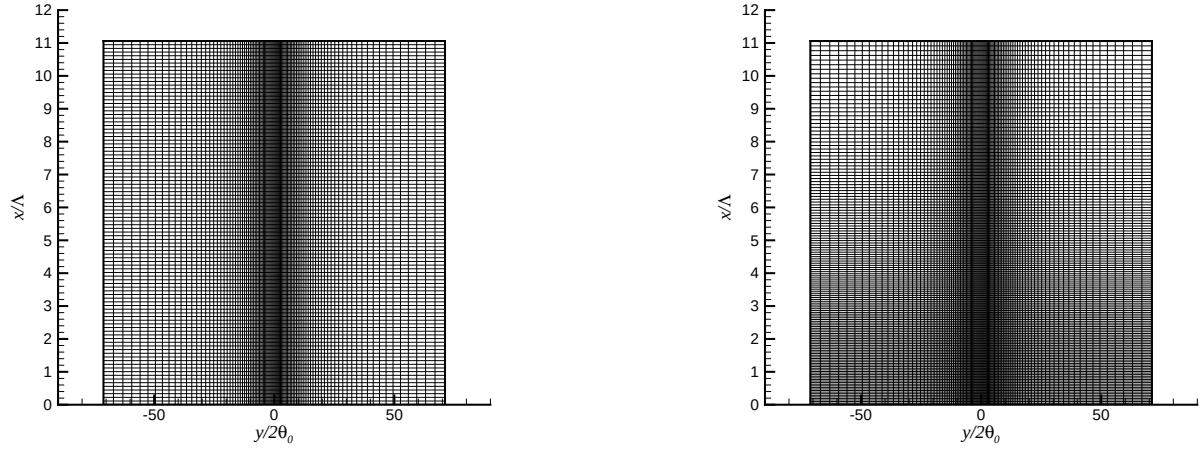

Figure 2. Examples of nonuniform grids used in planar mixing layer simulations.

An important part the validation procedure involves setting appropriate scalar artificial dissipation values. Its implicit coefficients control the pseudo-time convergence process, whereas their explicit counterparts control spurious oscillations in the dependent variables. The former has no impact on accuracy but the latter does, since central difference schemes do not introduce numerical dissipation. This can be observed in Figure 3, which shows decreased oscillations inside the mixing layer with increased numerical dissipation. Furthermore, these values are not high enough to modify the physically correct spatial gradients.

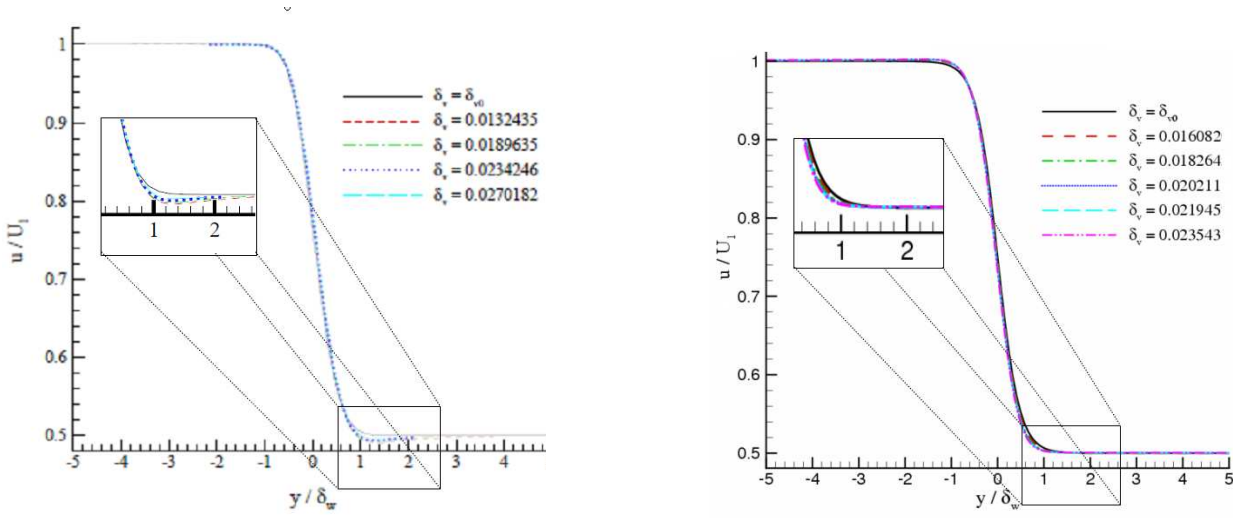

Figure 3. Streamwise velocity profiles normalized with respect to the local vorticity thickness for different AD_e with central difference of second order

Another important validation test is verifying if similarity holds for the streamwise velocity component. This can be done by re-plotting it at different downstream positions as a function of the cross-stream independent coordinate made dimensionless by the local vorticity thickness ($\delta_v \equiv (U_1 - U_2)/(du/dy)_{y=0}$). Figures 4 and 5 show these results for the second and fourth order simulations, respectively. In each figure, this velocity component is shown before and after being written in dimensionless form. It is clear that all profiles collapse under the same curve, demonstrating similarity. Furthermore, no oscillations are present.

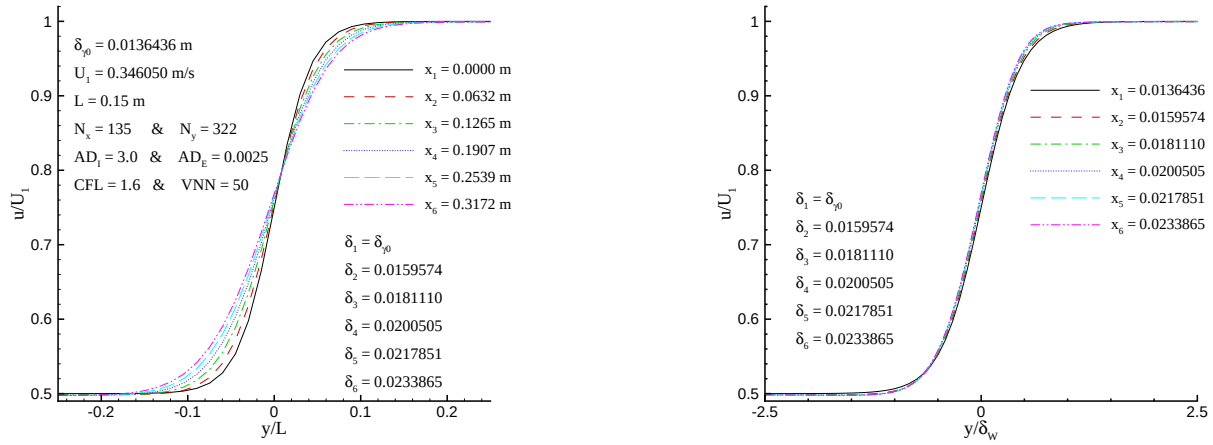

Figure 4. Normalized streamwise velocity profiles obtained from second-order code with nonuniform grid.

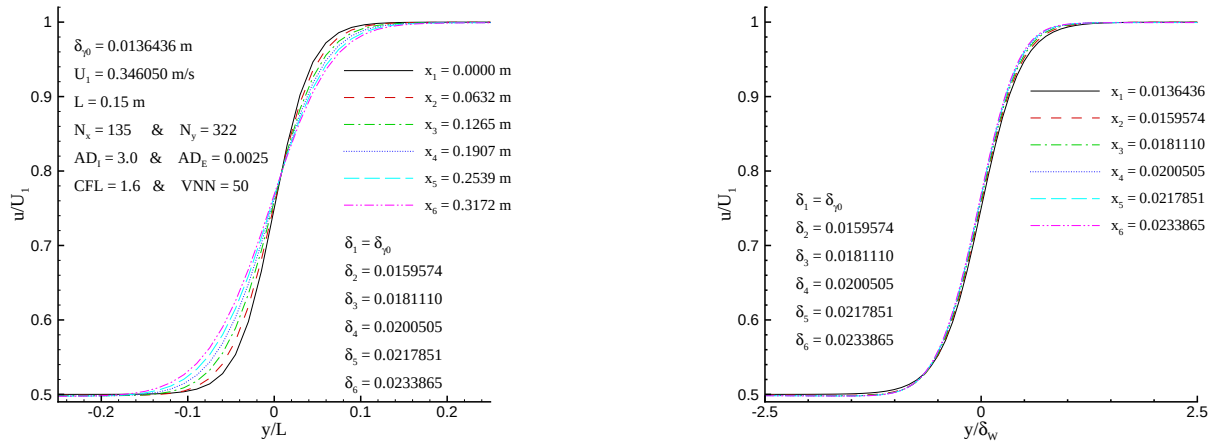

Figure 5. Normalized streamwise velocity profiles obtained from fourth-order code and nonuniform grid.

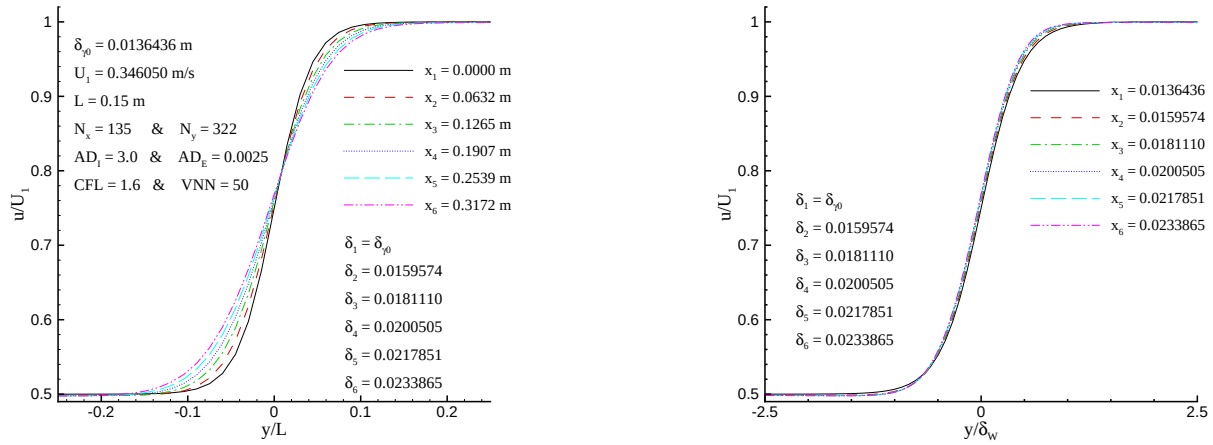

Figure 6. Normalized streamwise velocity profiles obtained from fourth-order code and uniform grid.

The same simulation is run on an uniform grid as a final test to verify solution accuracy. Its results are shown in Figure 6 and qualitative agreement can be observed. In order to quantify this accuracy evaluation, results from figures 4 and 5 are subtracted and shown in Figure 7. This difference is essentially an absolute error estimation for the second-order solution. It shows that $\max[\Delta p_g] \sim 4.49422 \times 10^{-4}$, nine orders of magnitude smaller than atmospheric pressure. Furthermore, $\max[\Delta v] \sim 5.79388 \times 10^{-4}$, one order of magnitude smaller than the maximum value for the cross-stream velocity component. These results are to be expected since pressure is constant for the similar solution and the cross-stream component obtained from the numerical simulation is not self-similar (Alston and Cohen, 1992).

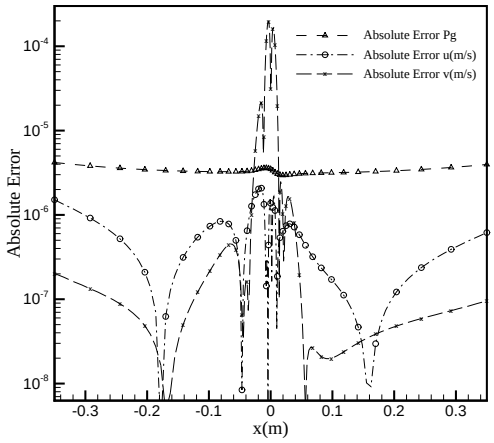

Figure 7. Absolute error estimate for second-order solution using fourth-order one.

Finally, the last analysis of the current paper looks into the number of pseudo-time iterations and maximum physical-time derivative with physical-time for simulations run with Mach numbers ranging from $M = 10^{-3}$ to 0.3. This study is presented in Figure 8 and demonstrates that steady-state solutions can be generated for a wide range of parameters.

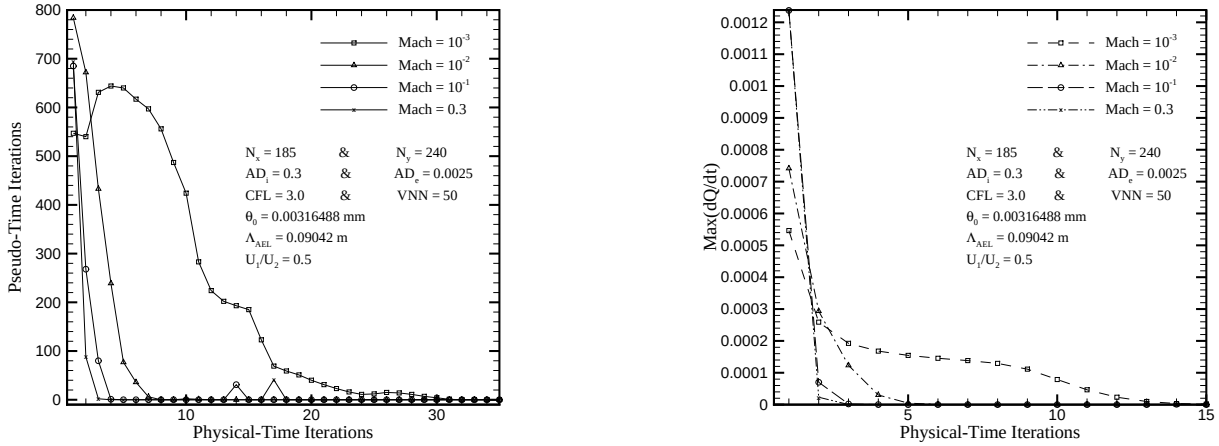

Figure 8. Pseudo-time iterations and steady-state convergence in physical-time.

4. CONCLUSIONS

A procedure is proposed in the present paper to generate high-order artificial steady-state solutions for a wide range of flow parameters. This is only possible because dual time stepping is used to introduce dissipation through a first-order approximation for the physical-time derivative term, which damps all disturbances that would otherwise grow and make this particular flow intrinsically unsteady. Furthermore, this procedure has no impact on steady-state spatial gradients. These solutions are going to be used as reference profiles for initial and boundary conditions in future unsteady simulations with high temporal resolution. Finally, the authors believe this procedure can be applied to arbitrary codes.

5. ACKNOWLEDGEMENTS

The authors would like to acknowledge the financial support of CAPES/Brazil and Instituto Militar of Engenharia.

6. REFERENCES

Alston, T. M. and Cohen, I. M., 1992, "Decay of a Laminar Shear-Layer", *Physics of Fluids*, Vol. 4, no. 12, pp. 1690–2699.

Alves, L. S. de B., 2006,"Transverse Jet Shear-Layer Instabilities: Linear Stability Analysis and Numerical Simulations", Ph.D. Thesis, University of California at Los Angeles.

Blaschak, J. G., Kriegsmann G. A., 1988, "A comparative Study of Absorbing Boundary Conditions", *Journal of Computational Physics*, Vol. 77, pp. 109-139.

Bodony, D. J., 2006, "An Analysis of Sponge Zones for Computational Fluid Mechanics", *Journal of Computational Physics*, Vol. 212(2), pp. 681 - 702.

Buell, J. C., Huerre, P., 1988, "Inflow and outflow boundary conditions and global dynamics of spatial mixing layer", Center for Turbulence Research, Stanford

Choi, Y. H., Merkle, C. L., 1993, "The Application of Preconditionig in Viscous Flows", *Journal of Computational Physics*, Vol. 105, pp. 207-223.

Colonius, T., Lele, K. S., Moin, P., 1993, "Boundary Conditions for Direct Computation of Aerodynamic Sound Generation", *Journal AIAA*, Vol. 31, No. 9.

Douglas, J., Gunn, J. E., 1964, "A General formulationof the alternating Directions implicit Method - Part I - Parabolic and Hyperbolic Problems". *Numerische and Mathematik*, Vol. 82, pp. 428-453.

Giles, M. B., 1990, "Nonreflecting boundary conditions for euler equations calculations", it AIAA Journal, Vol. 28, No. 12.

Grinstein, F. F., Oran, E. S., Boris, J. P., 1990, "Reinitiation and Feedback in Global Instabilities of Subsonic Spatially Developing Mixing Layers",*Physical Review Letters*, 64(8): 870 - 873.

Grosch, C. E., Orszag, S. A., 1977, "Numerical Solution of Problems in Unbounded Regions: Coordinate Transforms", *Journal of Computational Physics*, Vol. 25, pp. 273 - 296.

Poinsot, K. J., Lele, S. K., 1992, "Boundary Conditions of Direct Simulations of Compressible Viscous Flows," *Journal of Computational Physics*, Vol. 101, pp. 104-129.

Shuen, J. S., Chen, K. H., Choi, Y. H., 1992, "A Time-Accurate Algorithm for Chemical Non-Equilibrium Viscous Flows at All Speeds", *Journal of Computational Physics*, Vol. 106, pp. 306-318.

Shuen, J. S., Chen, K. H., Choi, Y. H., 1993, "A Coupled implicit Method for Non-Equilibrium Flows at All Speeds", *Journal of Computational Physics*, Vol. 106, pp. 306-318.

Tannehill, J. C., Anderson, D. A. and Pletcher, H. R., 1984, *Computational Fluid Mechanics and Heat Transfer*, Second Edition ,Taylot & Francis.

Teixeira, R. de S., Alves, L. S. de B., Karagozian, A. R., Kelly, R. E., 2008, "On the Solution of the Compressible Flow Equations at Small Mach Numbers", *Proceedings of the 12th ENCIT*, Paper 6-4743.

Thompson, K. W. , 1987, "Time Dependent Boundary Conditions for Hiperbolic Systems", *Journal of Computational Physics*, Vol. 68, pp. 1-24.

Venkateswaran, S., Merkle, C. L., Zeng, X. Q. and Li, D., 2002, "Influence of Large Scale Pressure Changes on Preconditioning Solutions at Low Speeds", AIAA Conference Paper, 2002-2957.

Zeng, X. Q. , Venkateswaran, S., Li, D. and Merkle, C. L., 2003, "Designing Dual-Time Algorithms for Steady-State Calculations", AIAA Conference Paper, 2003-3707.

7. Responsibility notice

The authors are the only responsible for the printed material included in this paper.